# Plasmonic enhanced quantum well infrared photodetector with high detectivity

Wei Wu,[a)] Alireza Bonakdar, and Hooman Mohseni[b)]
*Department of Electrical Engineering and Computer Science, Bio-inspired Sensors and Optoelectronics
Laboratory (BISOL), Northwestern University, Evanston, Illinois 60208, USA*

We report a normal-incident quantum well infrared photodetector (QWIP) strongly coupled with surface plasmon modes. A periodic hole array perforated in gold film was integrated with $In_{0.53}Ga_{0.47}As/InP$ QWIP to convert normal-incident electromagnetic waves into surface plasmon waves, and to excite the intersubband transition of carriers in the quantum wells. The peak responsivity of the photodetector at $\sim 8$ $\mu m$ was $\sim 7$ A/W at the bias of 0.7 V at 78 K with the peak detectivity as high as $\sim 7.4 \times 10^{10}$ cm Hz$^{1/2}$/W. The full width at half maximum of the response spectrum was only $\sim 0.84$ $\mu m$ due to a narrow plasmonic resonance. © *2010 American Institute of Physics.* [doi:10.1063/1.3419885]

Since Ebbesen *et al.*[1] found the extraordinary optical transmission of periodic metal nanohole arrays by surface plasmons, properties of surface plasmons have attracted a lot of research interests and been applied into many applications.[2] For example, surface plasmons have been used to improve the efficiency of optoelectronic devices such as solar cells,[3] light emitters,[4] semiconductor lasers,[5] and photodetectors.[6] Recently, periodic metal hole arrays have been applied to quantum dot infrared photodetectors to enhance the efficiency.[7,8] However, as far as we know, there is still no experimental study on applying surface plasmons to enhance the sensitivity of quantum well infrared photodetector (QWIP). Unlike quantum dot infrared photodetectors, QWIP is only sensitive to the electromagnetic (EM) waves which have electric field component normal to the quantum wells surface (TM mode).[9] In the mid and long-infrared wavelengths, where most QWIP devices are operational, the penetration depth of surface plasmons in metals is greatly reduced. Therefore, it yields a low optical loss, and surface plasmon waves have a long propagation length.[10] Surface plasmon supports TM mode and requires the electric field being normal to the surface because of the generation of surface charge.[11] In addition, a carefully designed plasmonic array forms standing waves and produces a cavity effect, which leads to an enhanced transverse plasmonic mode. Therefore, if properly coupled, surface plasmons can resonate with electron intersubband transitions, and efficiently excite carriers in the QWs to generate a strong photocurrent.

To simulate the surface plasmon waves and electric field component distribution we used three-dimensional finite-difference time-domain methods. The simulated structure is shown in Fig. 1(a), where the source is a normally incident plane wave. After optimizing the electric field intensity distribution at the wavelength of $\sim 8$ $\mu m$, where our QWIP device works, we selected the diameter of the holes $d$ as 1.4 $\mu m$, the lattice constant of the array $a$ as 2.9 $\mu m$, and the thickness of Au layer $t$ as 40 nm. The Au layer perforated with holes array is on top of $In_{0.53}Ga_{0.47}As/InP$ semiconductor layers. Figure 1(b) shows the simulated spectrum of $|E_z|^2$

averaged across the whole quantum well active region between 140 and 584.8 nm below the Au/Semiconductor interface [the exact structure is shown in Fig. 2(a)]. The values on the $y$-axis show the enhancement ratio of the averaged $|E_z|^2$ compared with $|E|^2$ for a structure without the surface plasmon layer. At the peak wavelength, the electric field enhancement ratio by the surface plasmons is more than five. The $E_z$ intensity ($|E_z|^2$) effectively represents the amount of light being absorbed by the detector, because QWIPs are only sensitive to electric field in the growth direction. The spectrum shows a strong resonance peak at the wavelength of $\sim 7.95$ $\mu m$ with the full width at half maximum (FWHM) of $\sim 0.84$ $\mu m$ or $\sim 16$ meV, which is due to the $(\pm 1, 0)$ surface plasmon mode on the Au/semiconductor interface. Figure 1(c) shows $|E_z|^2$ in the central plane of the active region at the peak absorption wavelength. The circles in the figure represent the positions of the holes perforated in the top Au film. Strong surface plasmon waves are generated in
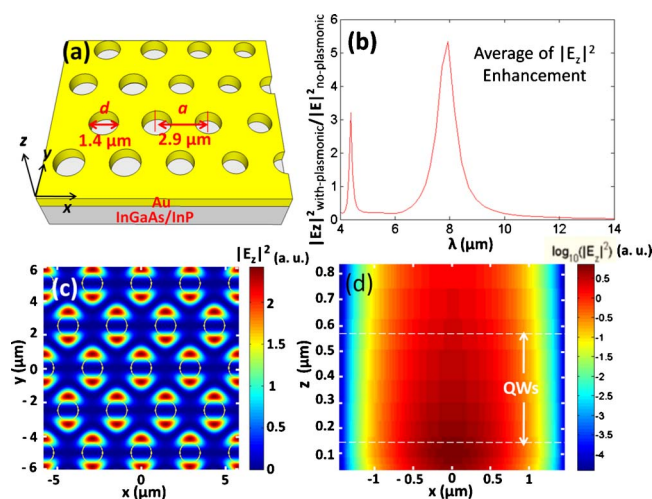


FIG. 1. (Color online) (a) A schematic of the simulated structure; (b) averaged $E_z$ intensity enhancement ratios in the quantum well active region compared with E intensity without surface plasmonic coupling at a normal incidence; (c) $E_z$ intensity in the x-y plane at the center of the active region at the peak absorption wavelength; (d) $E_z$ intensity in the x-z plane at the y point with the peak $E_z$ intensity at the peak absorption wavelength (the active region of quantum wells is between the white dash lines).

a)Electronic mail: wwu@u.northwestern.edu.
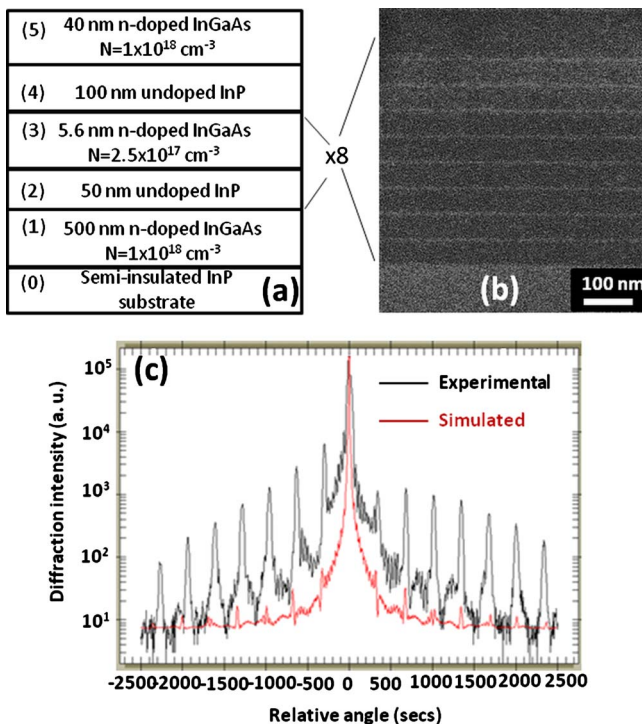b)Electronic mail: hmohseni@northwestern.edu.

FIG. 2. (Color online) (a) The growth structure of the QWIP; (b) SEM image of eight periods of quantum well active regions (the brighter region is the doped InGaAs layers); (c) simulated and experimental XRD curves of eight periods of quantum wells.
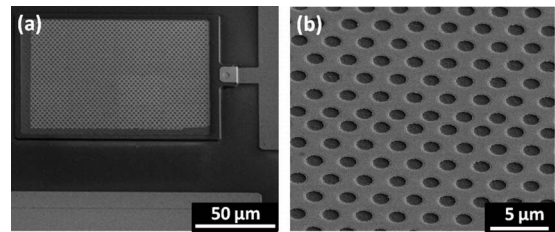


FIG. 3. (a) Fabricated QWIP device with periodic Au holes on the top of the mesa, the right pattern is connected to the top contact, and the lower pattern is connected to the bottom contact; (b) the enlarged oblique view of the periodic holes in Au film produced by FIB milling.

passivation layer of 360 nm $Si_xN_y$ was deposited on the sample by plasma-enhanced chemical vapor deposition. A thick Ti/Au layer (500 nm thick) was patterned besides the mesas and formed Ohmic contacts to the top of the mesa via a small opening in the $Si_xN_y$ layer. Below the mesa, another thick Ti/Au layer formed Ohmic contacts to the bottom of the mesas. On top of the mesas, $Si_xN_y$ layer was etched by reactive ion etching, and 40 nm thick Au layer was deposited by electron beam evaporation and patterned with periodic holes using focal ion beam (FIB) milling. A final device structure is shown in Fig. 3(a). On the right side of the mesa the metal is connected to the top $In_{0.53}Ga_{0.47}As$ layer forming the top contact, and the pattern below the mesa is connected to the bottom $In_{0.53}Ga_{0.47}As$ layer forming the ground contact. Both contacts are wire-bonded. Figure 3(b) is the SEM oblique view of the holes perforated in Au film on top of the mesa. The measured diameter $d$ of the hole is 1.4 $\mu$m, and the period $a$ of the array is 2.9 $\mu$m. The conditions of FIB milling were optimized to get a smooth edge of the holes and to minimize the damages of the semiconductor layers below. Other lithography techniques, such as super lens lithography,[13,14] can also be applied to generate these periodic hole arrays over large areas with a high throughput.

The dark current density-voltage curve of the device was characterized at 78 K and shown in Fig. 4. The dark current under a positive bias is smaller than that under a negative bias, which may be attributed to the asymmetrical $In_{0.53}Ga_{0.47}As/InP$ heterointerface.[15] The spectral response of the device was measured at 78 K using a Fourier transform infrared spectrometer (Thermo-Scientific Nicolet 6700) equipped with a cryostat and a calibrated HgCdTe (MCT) photodetector with peak detection wavelength of ~8.8 $\mu$m. The IR light source is normally incident on the front side of

the active region between the holes and the electric field component $E_z$ is greatly enhanced because of the surface plasmon generation. Figure 1(d) illustrates $|E_z|^2$ distribution in the x-z plane starting from the Au/semiconductor interface at the y point with the peak $|E_z|^2$. A large $E_z$ component almost covers the entire lattice period in the active region and the $E_z$ intensity is still very strong even at 800 nm below Au/semiconductor interface. Therefore, most of the quantum well active region can effectively receive and absorb the EM waves with a considerable $E_z$ component.

The device structure of the QWIP is illustrated in Fig. 2(a). The parameters of the quantum wells were selected to achieve a peak absorption wavelength ~8 $\mu$m with a bound-to-continuum transition.[12] The sample is grown by metal-organic chemical vapor deposition on a (001) oriented semi-insulating InP substrate. It includes eight periods of 5.6 nm thick $In_{0.53}Ga_{0.47}As$ quantum wells doped with Si to a concentration of $2.5 \times 10^{17}$ cm$^{-3}$ and 50 nm thick undoped InP quantum barriers. The quantum wells are sandwiched between two highly doped $In_{0.53}Ga_{0.47}As$ ($1 \times 10^{18}$ cm$^{-3}$) layers with the thicknesses of 40 and 500 nm separately for forming top and bottom Ohmic contacts. The quantum well region is designed to be very close to the top surface for maximized coupling with surface plasmon waves. Figure 2(b) is the high-resolution scanning electron microscope (SEM) image of the quantum well region. Figure 3(c) shows the x-ray diffraction (XRD) results of the grown layers after optimizing the growth conditions, which indicates the excellent uniformity, and control over layer thickness and material compositions. A large number of satellite peaks also indicate a high-quality growth of the materials. After the growth of the layers, the sample was defined into $130 \times 130$ $\mu$m$^2$ mesas by standard photolithography and chemical etching. A
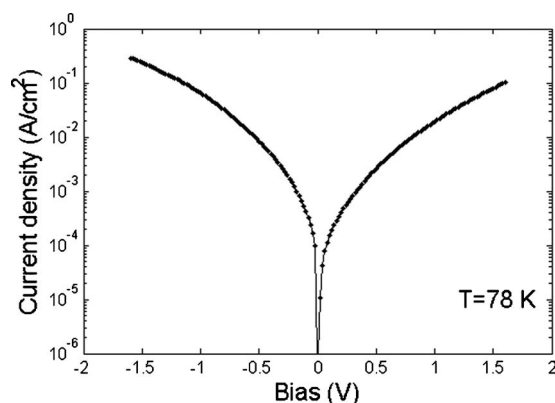


FIG. 4. The measured dark current density-voltage curve of the device at 78 K.
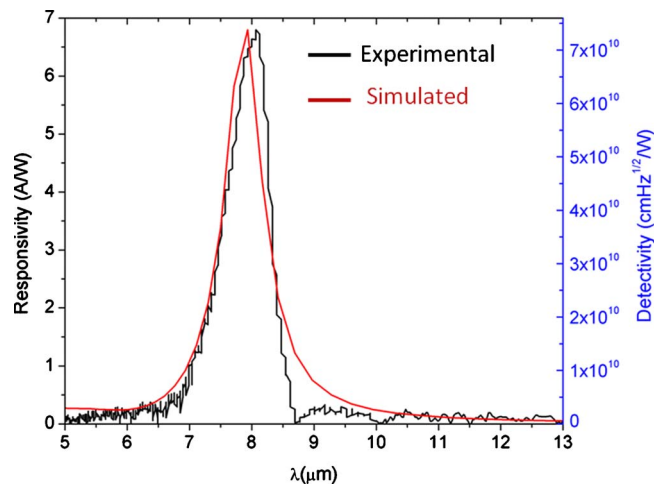
FIG. 5. (Color online) The measured responsivity (left) and detectivity (right) spectrum of the device at a normal-incident infrared radiation at the bias of 0.7 V at 78 K (the black curve) and the simulated averaged $E_z$ intensity spectrum (the red curve) in the quantum well active region.

the device patterned with Au holes arrays. Figure 5 illustrates the responsivity spectrum of the sample at 78 K and biased at 0.7 V. The peak responsivity of the sample occurs at ~8.06 $\mu$m and reaches a value as high as ~7 A/W. Using the measured dark currents and responsivity, the detectivity of the device was also calculated[9] (see the right axis of Fig. 5) and the peak value is ~7.4×10$^{10}$ cm Hz$^{1/2}$/W. This detectivity is a few times higher than other InP/In$_{0.53}$Ga$_{0.47}$As QWIP devices[16,17] working at a similar wavelength and temperature, because of the strong enhancement of $E_z$. The FWHM value of the spectrum is ~0.84 $\mu$m, which is almost half of the standard In$_{0.53}$Ga$_{0.47}$As/InP bound-to-continuum QWIP device.[12] We think the reason for such a narrow resonance is the strong modulation of the QWIP device by the surface plasmon resonance of the Au holes arrays. We compared the response spectrum (the black curve) with the simulated averaged $E_z$ intensity spectrum (the red curve), and the two spectra are almost identical as shown in Fig. 5. The narrow responsivity linewidth of the photodetector is beneficial to the applications that require high spectral resolution, while it may not be favorable for the broadband detection.

In conclusion, we demonstrated strongly coupled surface plasmon resonance modes with intersubband electron transitions in a QWIP device. The coupled QWIP works at normal light incidence, with an enhanced responsivity due to the plasmonic hole array. We believe this method provides an attractive way for fabrication of high performance infrared imagers.

[1] T. W. Ebbesen, H. J. Lezec, H. F. Ghaemi, T. Thio, and P. A. Wolff, Nature (London) **391**, 667 (1998).
[2] C. Genet and T. W. Ebbesen, Nature (London) **445**, 39 (2007).
[3] S. Pillai, K. R. Catchpole, T. Trupke, and M. A. Green, J. Appl. Phys. **101**, 093105 (2007).
[4] K. Okamoto, I. Niki, A. Shvartser, Y. Narukawa, T. Mukai, and A. Scherer, Nat. Mater. **3**, 601 (2004).
[5] A. Tredicucci, C. Gmachl, F. Capasso, A. L. Hutchinson, D. L. Sivco, and A. Y. Cho, Appl. Phys. Lett. **76**, 2164 (2000).
[6] Z. Yu, G. Veronis, S. Fan, and M. L. Brongersma, Appl. Phys. Lett. **89**, 151116 (2006).
[7] S. C. Lee, S. Krishna, and S. R. J. Brueck, Opt. Express **17**, 23160 (2009).
[8] C. Chang, H. Chang, C. Chen, M. Tsai, Y. Chang, S. Lee, and S. Tang, Appl. Phys. Lett. **91**, 163107 (2007).
[9] B. F. Levine, J. Appl. Phys. **74**, R1 (1993).
[10] A. C. Jones, R. L. Olmon, S. E. Skrabalak, B. J. Wiley, Y. N. Xia, and M. B. Raschke, Nano Lett. **9**, 2553 (2009).
[11] W. L. Barnes, A. Dereux, and T. W. Ebbesen, Nature (London) **424**, 824 (2003).
[12] Y. Gusakov, E. Finkman, G. Bahir, and D. Ritter, Appl. Phys. Lett. **79**, 2508 (2001).
[13] W. Wu, A. Katsnelson, O. G. Memis, and H. Mohseni, Nanotechnology **18**, 485302 (2007).
[14] W. Wu, D. Dey, A. Katsnelson, O. G. Memis, and H. Mohseni, J. Vac. Sci. Technol. B **26**, 1745 (2008).
[15] S. D. Gunapala, B. F. Levine, D. Ritter, R. Hamm, and M. B. Panish, Appl. Phys. Lett. **58**, 2024 (1991).
[16] O. O. Cellek, S. Ozer, and C. Besikci, IEEE J. Quantum Electron. **41**, 980 (2005).
[17] J. Y. Andersson, L. Lundqvist, Z. F. Paska, K. Streubel, and J. Wallin, Proc. SPIE **1762**, 216 (1992).